Microporous and Mesoporous Materials 181 (2013) 160–165

Contents lists available at ScienceDirect

Microporous and Mesoporous Materials

journal homepage: www.elsevier.com/locate/micromeso

Synthesis of wide spectrum of mesoporous titania materials by forced co-hydrolysis of Zr–Ti alkoxides

Maria Cristina Mascolo *

Laboratory of Materials – Department of Civil and Mechanical Engineering, University of Cassino and Southern Lazio, Via G. Di Biasio, 43 – 03043 Cassino, FR, Italy

ARTICLE INFO

Article history:
Received 3 August 2012
Received in revised form 21 May 2013
Accepted 12 July 2013
Available online 20 July 2013

Keywords:
Co-hydrolysis
Catalysts
ZrO_2 (5 mol%) incorporated titania
Macrosized mesoporous aggregates

ABSTRACT

A wide spectrum of mesoporous titania (TiO_2) materials has been synthesized by co-hydrolysis of titanium tetraethoxide in mixture with zirconium tetraisopropoxide (5 mol%) by changing the hydrolysis temperature, from 110 °C to 140 °C, the reaction time, from 20 h up to 144 h, the catalyst, NH_4OH or NH_4Cl, and the alcoholic media, ethanol or isopropanol. For short reaction times and/or for low temperatures of hydrolysis, micrometer aggregates of amorphous and microporous products were obtained. By increasing both the reaction time and temperature, the crystallization of TiO_2-anatase occurs with a strong change of micropores into mesopores.

In this work are discussed the numerous parameters which affect the crystallization of TiO_2, allowing to obtain a wide spectrum of mesoporous materials characterized by crystal sizes and average pore diameters ranging between 9 nm and 38 nm and from 2.5 nm to 16 nm, respectively.

© 2013 Elsevier Inc. All rights reserved.

1. Introduction

Mesoporous titanium dioxide (TiO_2) is intensively studied for its widespread applications in catalysis, gas sensor, photoelectrolysis, photocatalysis and as film working electrode for dye-sensitized solar cells (DSSC's) [1–6]. To enhance the efficiency for these applications, great efforts have been devoted to the structure and morphology of TiO_2 [7–9]. Shape and size of grains, high surface area and crystallinity, tailored pore network are the most important factors affecting such applications. Mesoporous titania with such factors is generally produced by the sol–gel method through the surfactant templating technology [10–18]. However, the resulting mesoporous products are generally poor crystallized and contaminated by the template. In order to enhance the crystallinity of TiO_2 and to remove the template, the products are submitted to heat treatment which frequently determines a partial or total collapse of mesopores with the consequent and dramatic reduction of the photo-catalytic activity. To stabilize the mesoporous structure of titania, a post treatment with bases has been adopted [19–21].

Mesoporous structures synthesized in the absence of a template have also attracted much attention [22–32]. They generally exhibit disordered macro-mesoporous structures owing to the aggregation of primary nanoparticles but the mechanism of the mesopores formation is not well understood.

To enhance the photocatalytic activity, research efforts have been also directed on different doping of mesoporous TiO_2 [33–43].

The nano-sized titania powder, used in wastewater treatment process, has a problem in its recycle-ability. For this purpose, supporting materials coated with mesoporous TiO_2 have been developed [44–46]. The consequent surface area reduction of the nano-scale TiO_2 determines a diminution of its photo-catalytic efficiency. To avoid such an inconvenient, macro-sized aggregates of TiO_2 with low ordered mesoporous structure, were obtained in the presence [47] or in the absence of a template [48]. As the high ordered mesoporous structure of titania does not appear a prerequisite for high photocatalytic activity [6] and taking into account the macro-scale aggregates of disordered mesoporous ZrO_2 (5 mol%)-TiO_2 synthesized by co-hydrolysis of Zr–Ti alkoxides in the absence of a template [48], further experimentals have been performed. The objective is that to elucidate the mechanism of mesopores formation in order to produce nanometric products as aggregates micrometer in size characterized by high crystallinity and mesoporosity.

2. Experimental

Mixtures of titanium tetraethoxide, ($Ti(OC_2H_5)_4$), and zirconium tetraisopropoxide, ($Zr(OC_3H_7)_4$), (R.G. Aldrich) were used for preparing ZrO_2 (5 mol%) incorporated TiO_2 materials by forced co-hydrolysis. The detailed experimental conditions for the syntheses have been carried out according to the procedures mentioned in [48]. The products synthesized by changing the various parameters are listed in the Table 1. The syntheses were performed

* Tel.: +39 07762994346; fax: +39 07762993711.
E-mail address: mc.mascolo@unicas.it

1387-1811/$ - see front matter © 2013 Elsevier Inc. All rights reserved.
http://dx.doi.org/10.1016/j.micromeso.2013.07.021

Table 1
Characteristics of the products obtained by co-hydrolysis in ethanol or isopropanol of Ti-tetraethoxide in mixture with Zr-tetraisopropoxide (5 mol%) and catalyzed by NH_4OH or by NH_4Cl for different hydrolysis temperature and time duration, respectively.

Hydrolysis temperat./time duration (°C/h)	Alcoholic media	Catalyst	Crystallinity	Pore volume (cm^3/g)	BET surface area (m^2/g)	Average pore diameter (nm)	Average crystal size (nm)
110/20	Ethanol	NH_4OH	Amorphous	–	–	–	–
110/48	Ethanol	NH_4OH	Amorphous	–	–	–	–
110/96	Ethanol	NH_4OH	Amorphous	–	–	–	–
110/144	Ethanol	NH_4OH	Amorphous	0.41	551	2.1	–
120/20	Ethanol	NH_4OH	Amorphous	–	–	–	–
120/48	Ethanol	NH_4OH	Amorphous	–	–	–	–
120/96	Ethanol	NH_4OH	Poor cryst.	–	–	–	–
120/144	Ethanol	NH_4OH	Poor cryst.	0.37	323	3.2	18.6
130/20	Ethanol	NH_4OH	Poor cryst.	–	–	–	–
130/48	Ethanol	NH_4OH	Poor cryst.	0.39	362	2.7	19.5
130/96	Ethanol	NH_4OH	Full cryst.	–	–	–	–
130/144	Ethanol	NH_4OH	Full cryst.	0.48	144	9.3	20.9
140/20	Ethanol	NH_4OH	Poor cryst.	0.37	408	2.5	20.7
140/48	Ethanol	NH_4OH	Full cryst.	0.41	171	6.9	22.3
140/96	Ethanol	NH_4OH	Full cryst.	0.47	166	8.4	26.2
140/144	Ethanol	NH_4OH	Full cryst.	0.44	117	11.0	28.4
110/144	Isoprop.	NH_4OH	Amorphous	–	–	–	–
120/48	Isoprop.	NH_4OH	Poor cryst.	–	–	–	–
120/96	Isoprop.	NH_4OH	Poor cryst.	–	–	–	–
120/144	Isoprop.	NH_4OH	Full cryst.	0.48	113	12.0	30.1
130/20	Isoprop.	NH_4OH	Poor cryst.	–	–	–	–
130/48	Isoprop.	NH_4OH	Full cryst.	–	–	–	–
130/96	Isoprop.	NH_4OH	Full cryst.	0.44	140	8.3	30.4
130/144	Isoprop.	NH_4OH	Full cryst.	0.41	86	13.6	31.2
140/20	Isoprop.	NH_4OH	Poor cryst.	0.71	520	3.9	24.4
140/48	Isoprop.	NH_4OH	Full cryst.	0.40	124	10.1	27.4
140/96	Isoprop.	NH_4OH	Full cryst.	0.49	109	16.1	33.5
140/144	Isoprop.	NH_4OH	Full cryst.	0.34	71	15	37.3
120/20	Ethanol	NH_4Cl	Poor cryst.	–	–	–	–
120/48	Ethanol	NH_4Cl	Poor cryst.	–	–	–	–
120/96	Ethanol	NH_4Cl	Full cryst.	0.32	196	4.3	9.2
120/144	Ethanol	NH_4Cl	Full cryst.	0.30	183	4.5	9.5
140/20	Ethanol	NH_4Cl	Poor cryst.	0.29	290	2.7	8.1
140/48	Ethanol	NH_4Cl	Full cryst.	0.27	177	4.6	9.9
140/96	Ethanol	NH_4Cl	Full cryst.	0.28	179	4.8	10.4
140/144	Ethanol	NH_4Cl	Full cryst.	0.29	178	4.9	11.1

Poor cryst. = poor crystallized; Full cryst. = full crystallized; Isoprop. = Isopropanol.

in ethanol or isopropanol, catalyzed by NH_4OH or by NH_4Cl and by changing both the temperature and duration of hydrolysis, respectively. After the hydrolysis treatments performed in ethanol, the products were washed with ethanol, while the ones hydrolyzed in isopropanol were washed in isopropanol. The so treated products were dried in air at room temperature.

In order to investigate the effect of the nature of the washing liquid on the textural properties of the hydrolyzed products, some of them were washed with deionized water or with alcohol and after dried in air at room temperature.

Powder X-ray diffraction (XRD) measurements were taken using a Philips XL 30 powder diffractometer with Cu-Kα. The samples were scanned over the 2θ range of 10–80° (step time 10 s; step size 0.05°). The average diameter of the crystallites for the products was derived from the line broadening (1 0 1) peak of anatase of the corresponding XRD pattern according to the Debye–Scherrer equation.

The BET surface area of products was determined by nitrogen physic-sorption data measured at 77 K using a Gemini of Micromeritics after products were vacuum-dried at 453 K for 12 h. N_2 adsorption-desorption isotherms were used either to discriminate the presence of mesopores or to determine the average pore size using the BJH method.

3. Results and discussion

In the Table 1 are summarized the various parameters adopted for the forced hydrolysis of titanium tetraethoxide in mixture with zirconium tetraisopropoxide (5 mol%). Some characteristics of all the synthesized products, such as pore volume, BET surface area, average pore diameter and crystal sizes determined by XRD patterns, are also reported. Obviously, high BET surface areas result for the amorphous and poor crystallized products, while lower surface areas characterize the well crystallized samples. The XRD reflection peaks of these crystallized products, compared with the diffraction data of anatase TiO_2 (JPCDS card no. 21-1272), are the characteristic peaks of the anatase phase. This means that the incorporation of 5 mol% of ZrO_2 into TiO_2 does not change the structure of anatase-TiO_2. Such incorporation leads only to the shift of the XRD reflections to lower angles corresponding to the unit cell expansion due to the replacement of Ti^{4+} ions (radius 60.5 pm) by larger Zr^{4+} ions (radius 84.0 pm). The angle of 25.28° (2θ) for the plane (1 0 1) of pure anatase shifts, in fact, to 25.16°.

In Fig. 1 are resumed the effects of the various parameters on the crystallization of anatase. Each curve separates the full crystallization field of the products from that of amorphous or poor crystallized ones as function of the hydrolysis time as well as of the hydrolysis temperature. The full crystallization of anatase for the products catalyzed by NH_4OH in ethanol, curve *a*, requires longer reaction times and/or higher temperatures (30 h at 140 °C or 144 h at 125 °C), while lower values (30 h at 130 °C or 144 h at 115 °C) are necessary for the crystallization of products catalyzed by NH_4Cl in ethanol (curve *c*). Intermediate reaction times as well as hydrolysis temperatures need for the full crystallization of products catalyzed by NH_4OH in isopropanol (curve *b*). The length of the hydrolysis time as well as the increase of the hydrolysis

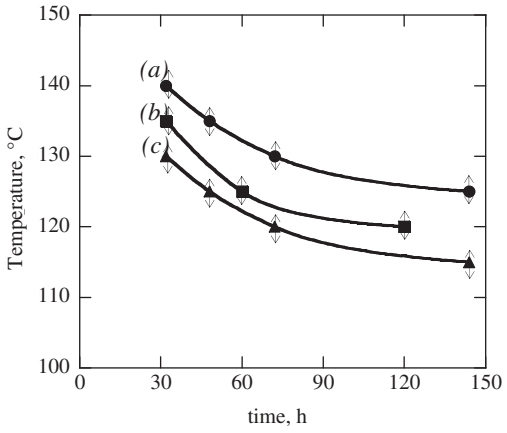


Fig. 1. Separation curves between the full crystallization field from that of amorphous or poor crystallized anatase for the products hydrolyzed in the presence of ethanol-NH_4OH (a), isopropanol-NH_4OH (b) and ethanol-NH_4Cl (c).

temperature significantly enhance the crystallization of anatase. A strong change in the surface area, from the wide range of 290–550 m^2/g to that of 72–178 m^2/g, is related to the evolution from the amorphous or poor crystallized products into well crystallized ones (Table 1).

The XRD peaks (1 0 1) of anatase for the full crystallized products synthesized at 140 °C and after the longest hydrolysis time of 144 h, are shown in Fig. 2. The different line broadening of the products indicate different crystal sizes of anatase. The (1 0 1) peak of the product catalyzed by NH_4Cl in ethanol is relatively broader (Fig. 2a) than the peak of the product catalyzed by NH_4OH in ethanol (Fig. 2b). That is attributable to the smaller particles size (8.1–11.1 nm) of the products catalyzed by NH_4Cl as confirmed by the Debye–Scherrer equation (Table 1). The finer crystals sizes for these products can justified by two concomitant effects: firstly, the NH_4Cl catalyst favors a faster crystallization rate of anatase; secondly, the acidic NH_4Cl produces positive charge onto the primary particles and, moreover, the adsorption of NH_4^+ cations on the particle surface [40] reduces the collisions among the primary particles, slowing their crystal growth. The same peak of anatase for products crystallized in isopropanol and catalyzed by NH_4OH (Fig. 2c) is relatively sharper than the peak of the products hydrolyzed in ethanol. Such finding justifies the greater crystal size of anatase for the product synthesized in isopropanol (24.4–37.3 nm) compared with that of the product synthesized in ethanol (18.6–28.4 nm, Table 1). The destabilizing effect of isopropanol on the colloidal particles [49] and the lower reactivity towards hydrolysis as the alkoxy chain length increases explain the enhanced crystal growth for products hydrolyzed in isopropanol [50].

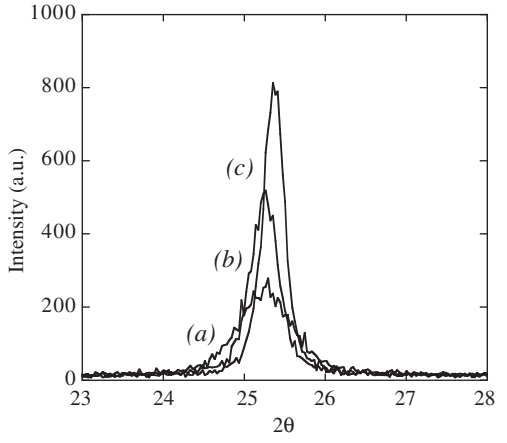


Fig. 2. XRD (1 0 1) peak of anatase, TiO_2, for the crystallized products at 140 °C for 144 h in the presence of NH_4Cl-ethanol (a), NH_4OH-ethanol (b) and NH_4OH–isopropanol (c).

The textural properties of the hydrolyzed products have been studied by the N_2 adsorption–desorption isotherms and the average pore diameter were obtained from BJH method based on desorption branches of the isotherms. The effects of the length of the hydrolysis time as well as the increase of the hydrolysis temperature on the textural properties of products catalyzed by NH_4OH in ethanol, are shown in Fig. 3. The resulting amorphous product hydrolyzed at room temperature for 1 h shows a typical IUPAC I-type isotherm which is a characteristic of the microporous solids with a strong adsorption of N_2 at the lowest relative pressure P/P_0 (Fig 3a). The sample hydrolyzed at 140 °C for 20 h, which resulted poor crystallized, Fig. 3b, shows a typical IV-type isotherm with type H_4 hysteresis loop in the 0.4–0.95 range of relative pressure and a corresponding reduction of the adsorption of N_2 at the lowest relative pressure P/P_0 That involves a reduction of the micropores and the formation of disordered mesopores characterized by a wide range of sizes. After 144 h of the duration of the hydrolysis reaction, (Fig. 3c), a further reduction of adsorption of N_2 at the lowest P/P_0 and a type H_3 isotherm with a hysteresis loop shifted at 0.8–1.0 range of relative pressure, have been detected. These results can be justified by further reduction of the micropores and formation of the mesopores with average pore diameter changing from 2.5 nm to 11.0 nm.

A comparison among the full crystallized products hydrolyzed under comparable conditions (140 °C for 144 h) in ethanol or isopropanol and in the presence of different catalyst, is reported

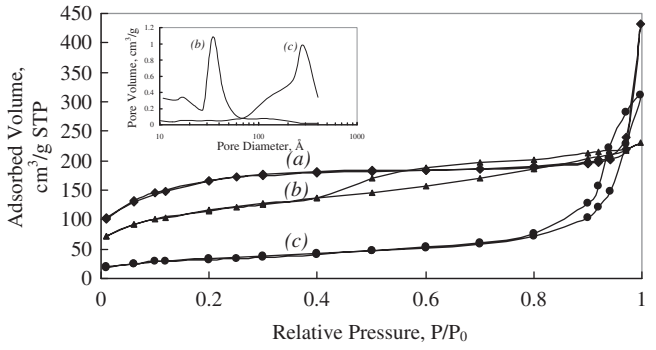


Fig. 3. N_2 Adsorption-desorption isotherms and pore size distributions of the products catalyzed by NH_4OH in the presence of ethanol at room temperature for 1 h (a), at 140 °C for 20 h (b) and at 140 °C for 144 h (c).

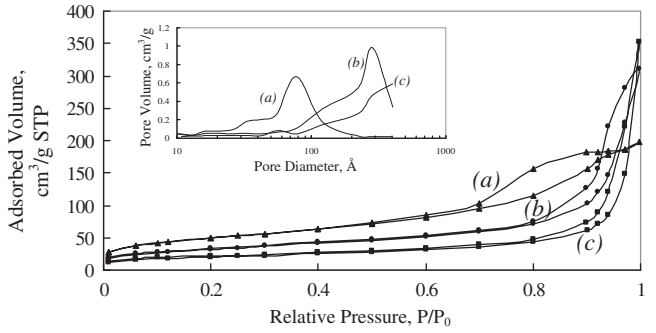


Fig. 4. N_2 Adsorption-desorption isotherms and pore size distributions of the products hydrolyzed at 140 °C for 144 h in the presence of NH_4Cl-ethanolo (a), NH_4OH-ethanol (b) and NH_4OH-isopropanol (c).

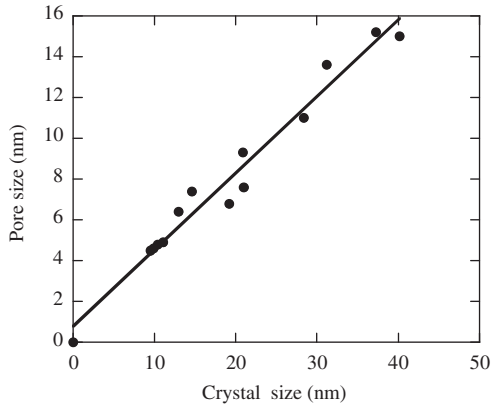


Fig. 5. Average mesopore size as a function of crystal size of anatase-TiO_2 for full crystallized products either calcined or not.

in Fig. 4. The product catalyzed by NH4Cl in ethanol, presents hysteresis loop in the 0.7–0.95 P/P_0 range (Fig. 4a) corresponding to mesopores with average pore diameter of 4.9 nm as a direct consequence of the smaller particles sizes of anatase (11.1 nm) as detected from XRD data (Table 1). The product hydrolyzed in isopropanol and catalyzed by NH4OH (Fig. 4c), exhibits hysteresis loop in the 0.8–1.0 $P/P0$ range due to larger mesopores (15.2 nm) as a consequence of their larger crystal sizes (37.3 nm).

Analogous hysteresis loop with a same type H_3 isotherm (Fig. 4b) can be observed for the product hydrolyzed in ethanol and catalyzed by NH4OH. In this case intermediate mesopore size according to the intermediate crystal size (Fig. 4b) resulted.

All the well crystallized products hydrolyzed at different temperatures and reaction times calcined or not display a direct correlation between the average pore diameter and their crystal sizes, as can be seen in Fig. 5.

As the formation of the mesopores in the products is connected to the crystallization of anatase, taking into account the correlation between the average pore diameter of mesopores and their crystal sizes, the textural properties of the hydrolyzed products can be planned through the crystallization process of anatase.

The following mechanism can be advanced for the formation of mesoporous aggregates of TiO_2 anatase. The first step involves the formation of nuclei of hydrous titania followed by their coarsening to form nano-sized spherical and amorphous particles characterized by a strong microporosity (SEM micrography of Fig 6a). Under continuous stirring the coarsening of these particles produces micrometer and amorphous aggregates, different in shape and size, containing numerous micropores and some mesopores (Fig. 6b). The forced step of the hydrolysis reaction, at higher temperature and/or for long time, determines the crystallization of amorphous hydrous titania into crystalline anatase involving a strong reduction of the micropores and a concomitant formation of the mesopores (Fig. 6c). The SEM micrographs of this morphological evolution, concerning the product catalyzed by NH_4OH in ethanol, show that after the crystallization of anatase there is not any significant change in the size and shape of the aggregates.

The effects of the calcination on the textural properties of some of the hydrolyzed products before and after the calcination are shown in Table 2. The calcination improves the crystallinity especially for poor crystallized samples, while the surface area drastically decreases and the average pore size increases.

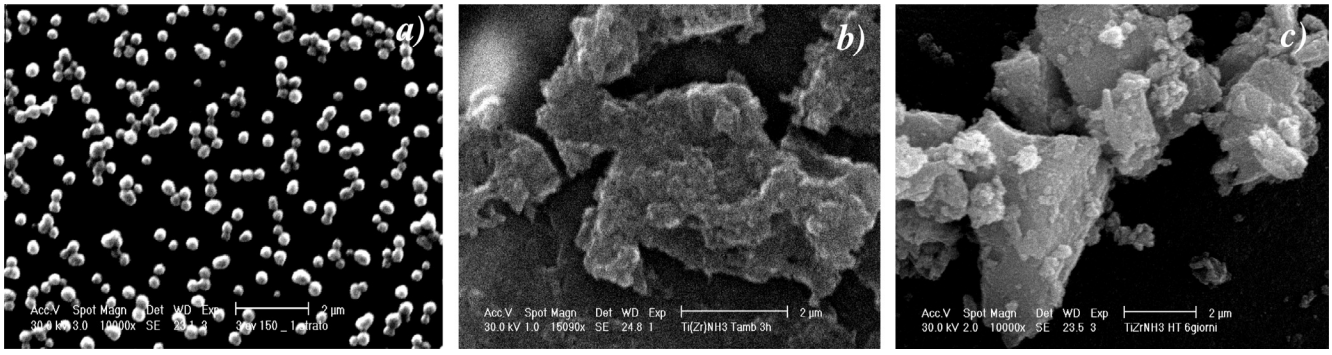


Fig. 6. SEM micrographs of products catalyzed by NH_4OH in the presence of ethanol at room temperature for 1 h (a), at room temperature for 3 h (b) and at 140 °C for 144 h (c).

Table 2
Comparison of the characteristics of some hydrolyzed products before and after calcination at 400 °C for 2 h.

Hydrolysis temperat./time duration (°C/h)	Alcoholic media	Catalyst	Crystallinity	Pore volume (cm^3/g)	BET surface area (m^2/g)	Average pore diameter (nm)	Average crystal size (nm)
120/144	Ethanol	NH_4OH	Poor cryst.	0.37	323	3.2	18.6
120/144c	Ethanol	NH_4OH	Full cryst.	0.34	118	7.6	21.0
130/48	Ethanol	NH_4OH	Poor cryst.	0.39	362	2.7	19.5
130/48c	Ethanol	NH_4OH	Full cryst.	0.32	125	6.8	19.2
140/144	Isoprop.	NH_4OH	Full cryst.	0.34	72	15.2	37.3
140/144c	Isoprop.	NH_4OH	Full cryst.	0.34	72	15.0	40.2
140/20	Ethanol	NH_4Cl	Poor cryst.	0.29	290	2.7	8.1
140/20c	Ethanol	NH_4Cl	Full cryst.	0.24	119	6.4	13.0
140/48	Ethanol	NH_4Cl	Full cryst.	0.27	177	4.6	9.9
140/48c	Ethanol	NH_4Cl	Full cryst.	0.28	106	7.4	14.6
140/144	Ethanol	NH_4Cl	Full cryst.	0.29	178	4.9	11.1
140/144c	Ethanol	NH_4Cl	Full cryst.	0.30	108	7.9	13.9

Poor cryst. = poor crystallized; Full cryst. = full crystallized; Isoprop. = Isopropanol; c = calcined at 400 °C for 2 h.

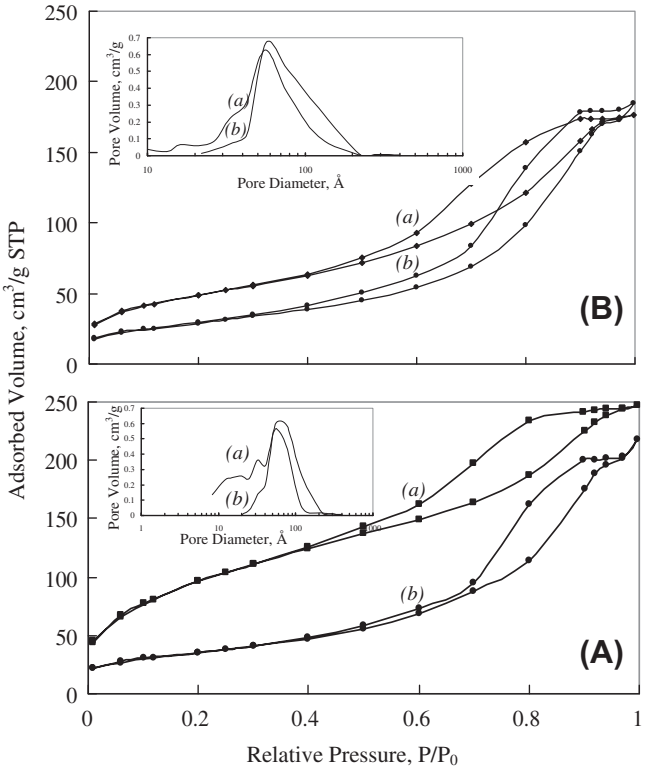


Fig. 7. N_2 Adsorption-desorption isotherms and pore size distributions of the products before (a) and after calcination (b). The figure (A) refers to the sample hydrolyzed at 130 °C for 48 h and catalyzed by NH_4OH in ethanol; the figure (B) refers to the sample hydrolyzed at 140 °C for 48 h and catalyzed by NH_4Cl in ethanol.

Generally, the thermal treatment of amorphous or poor crystallized products determines a conspicuous collapse of the micropores with a consequent increase in the average pore size. Such effect can be seen in Fig. 7A by comparing, before (a) and after calcination (b), the N_2 adsorption-desorption isotherms of the poor crystallized product hydrolyzed at 130 °C for 48 h and catalyzed by NH_4OH in ethanol. A drastic reduction of the N_2 adsorption at the lowest relative pressure can be seen, in fact, for the thermally treated sample, while no significant shift results for the relative pressure P/P_0 range connected to the hysteresis loop. The calcination of the full crystallized sample hydrolyzed at 140 °C for 48 h and catalyzed by NH_4Cl in ethanol, determines a small reduction of the N_2 adsorption at the lowest relative pressure (Fig. 7B) and an analogous and negligible shift of the relative pressure P/P_0 range connected to the hysteresis loop. This last feature involves any significant change of the size and the distribution of the mesopores on calcination.

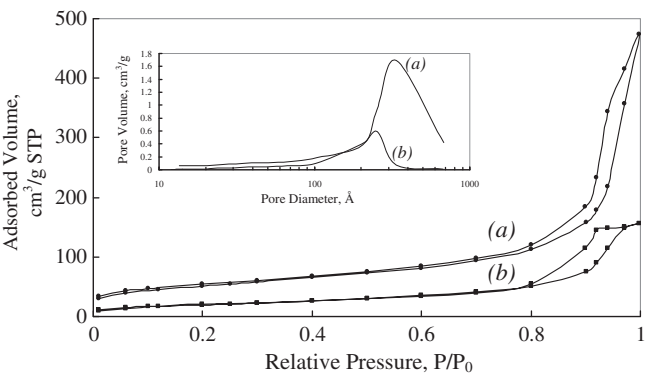


Fig. 8. N_2 Adsorption-desorption isotherms and pore size distributions of the product hydrolyzed at 120 °C for 144 h in the presence of NH_4Cl-isopropanol and washed with de-ionized water (a) or with isopropanol (b).

The textural properties of the hydrolyzed products are also affected by the nature of the washing liquid. Fig. 8 shows the N_2 adsorption-desorption isotherms for the sample hydrolyzed at 120 °C for 144 h and catalyzed by NH_4Cl in ethanol and washed with de-ionized water (curve *a*) or with ethanol (curve *b*) respectively and afterward dried in air at room temperature. The hydrolyzed product washed with de-ionized water results more rich in micropores and mesopores than that washed with ethanol. On the other hand the two samples contain mesopores different in shape. The influence of the washing liquid on the textural properties of the products can be explained by the effect of drying stresses. While drying, the primary nanoparticles of the products are forced by the drying stresses to come together [51]. The magnitude of the drying stress, originating from the capillary pull of the pore fluid, is directly proportional to the surface tension of the pore fluid and to the reciprocal of the pore radii. A greater drying stress must be expected when the pore fluid is water characterized by a high surface tension so favouring the formation of micropores for the products washed with de-ionized water in comparison with the same product washed with ethanol, which has a lower surface tension.

4. Conclusions

In the absence of a template and in a single step, a wide spectrum of mesoporous ZrO_2 (5 mol%)-TiO_2 products have been synthesized by forced co-hydrolysis of Ti-Zr alkoxides. The wide range of the mesopore sizes is a direct function of the crystal sizes of anatase as a consequence of the numerous parameters which affect its crystal growth.

The crystal size of anatase can be programmed by changing parameters such as, hydrolysis temperature, hydrolysis time, the catalyst, the alcoholic media, the washing liquid of the hydrolyzed products and the calcination temperature.

The co-hydrolysis catalyzed by NH_4OH in the presence of isopropanol favors products characterized by crystals of anatase as well as mesopores both larger in size than those catalyzed by NH_4OH in the presence of ethanol.

Products characterized by crystals and mesopores both smaller in sizes result in performing the hydrolysis catalyzed by NH_4Cl in the presence of ethanol in comparison to catalyzed by NH_4OH.

The calcination treatment of products determines a reduction of both the surface area and the microporosity, especially for the poorly crystallized products, while the calcination performed on the well crystallized products has a little influence on their textural properties.

A performing feature of the synthesized products concerns their macro-scale dimension as aggregates easier to recycle in catalysis applications.

References

[1] C.T. Kresge, M.E. Leonowicz, W.J. Roth, J.C. Vartuli, J.S. Beck, Nature 359 (1992) 710–712.
[2] X. Chen, S.S. Mao, Chem. Rev. 107 (2007) 2891–2959.
[3] Y.C. Nah, I. Paramasivam, P. Schmuki, Chem. Phys. Chem. 11 (2010) 2698–2713.
[4] S.A. Davis, S.L. Burkett, N.H. Mendelson, S. Mann, Nature 385 (1997) 420–423.
[5] W.S. Chae, S.W. Lee, Y.R. Kim, Chem. Mater. 17 (2005) 3072–3074.
[6] A.A. Ismail, D.W. Bahnemann, J. Mater Chem. DOI:10.1039/cc1jm10407a.
[7] H.X. Li, Z.F. Bian, J. Zhu, D.Q. Zhang, G.S. Li, Y.N. Huo, H. Li, Y.F. Lu, J. Am. Chem. Soc. 129 (2007) 8406–8407.
[8] L. Xu, C.Q. Tang, J. Quian, Z.B. Huang, Appl. Surf. Sci. 256 (2010) 2668–2671.

[9] S.L. Oh, K.H. Choi, J.E. Im, K.K. Wang, H.Y. Yaung, K.K. Kim, Y.R. Kim, Nanotechnology 22 (2011) 275309–275315.
[10] D.M. Antonelli, J.Y. Ying, Angew. Chem. Int. Ed. Engl. 34 (1995) 2014–2017.
[11] H. Yoshitake, T. Sugihara, T. Tatsumi, Chem. Mater. 14 (2002) 1023–1029.
[12] S. Cabrera, J.E. Jaskouri, A. Beltràn-Porter, D. Beltràn-Porter, D.D. Marcos, P. Amoròs, Solid State Sci. 2 (2000) 513–518.
[13] P. Yang, D. Zhao, D.I. Margolese, B.F. Chmelka, G.D. Stucky, Chem. Mat. 11 (1999) 2813–2826.
[14] L. Wang, S. Tomura, M. Maeda, F. Ohashi, K. Inukai, M. Suzuki, Chem. Lett. (2000) 1414–1415.
[15] H. Hao, J. Zhang, Mat. Lett. 63 (2009) 106–108.
[16] J. Orillal, M.C. Warrwn, S.C. Kamperman, M. Disalvo, F.J.U. Wiesner, Nat. Mater. 7 (2008) 222–228.
[17] M. Niederberger, M.H. Bartl, G.D. Stucky, Chem. Mater. 14 (2002) 4364–4370.
[18] G. Goutailler, C. Guillard, S. Daniele, L.G. Hubert-Pfalzgraf, J. Mater. Chem. 13 (2003) 342–346.
[19] D. Grosso, Adv. Mater. 13 (2001) 1085–1090.
[20] E. Beyers, P. Cool, E.F. Vansant, Microporous Mesoporous Mater. 9 (2007) 112–117.
[21] K. Cassiers, T. Linsen, M. Mathieu, Y.Q. Bai, H.Y. Zhu, P. Cool, E.F. Vansant, J. Phys. Chem. B 108 (2004) 3713–3721.
[22] B. Rajesh, N.R. Sasirekha, Y.W. Chen, Mater. Res. Bull. 43 (2008) 682–689.
[23] I. Kartini, P. Meredith, J.C. Diniz Da Costa, G.Q. Lu, J. Sol–Gel Technol. 31 (2004) 185–189.
[24] W. Ren, Z. Ai, F. Jiu, L. Zhang, X. Fan, Z. Zou, Appl. Catal. B Environ. 69 (2007) 139–144.
[25] A.H. Sun, P.J. Guo, Z.X. Li, Y. Li, P. Cui, J. Alloys Compd. 481 (1–2) (2009) 605–609.
[26] K.S. Yoo, T.G. Lee, J. Kim, Microporous Mesoporous Mater. 84 (1–3) (2005) 211–217.
[27] G. Li, J. Liu, G. Jiang, Chem. Commun. 47 (2011) 7443–7445.
[28] J.Y. Zheng, K.Y. Qiu, Y. Wei, J. Mater. Sci. 38 (2003) 437–444.
[29] H. Hayashi, K. Torii, J. Mater. Chem. 12 (2002) 3671–3676.
[30] V. Kolen'ko, V.D. Maximov, A.V. Garshev, P.E. Meskin, N.N. Oleynikov, B.R. Churagulov, Chem. Phys. Lett. 388 (2004) 411–414.
[31] S.W. Yang, L. Gao, J. Am. Ceram. Soc. 88 (2005) 968–970.
[32] J. Yang, S. Mei, J.M.F. Ferreira, J. Am. Ceram. Soc. 84 (2001) 1696–1702.
[33] J.C. Yu, J. Lin, R.W.M. Kwok, J. Phys. Chem. B 102 (1998) 5094–5098.
[34] H. Zou, Y.S. Lin, Appl. Catal. A Gen. 265 (2004) 35–42.
[35] Y. Huang, W. Ho, S. Lee, L. Li, G. Zhang, J.C. Yu, Langmuir 24 (2008) 3510–3516.
[36] J.C. Yu, J.G. Yu, W.K. Ho, Z.T. Jiang, L.Z. Zhang, Chem. Mater. 14 (2002) 3808–3816.
[37] S. Tojo, T. Tachikawa, M. Fujitsuka, T. Majima, J. Phys. Chem. C 112 (2008) 14948–14954.
[38] A.K. Sinha, K. Suzuki, J. Phys. Chem. B 109 (2005) 1708–1714.
[39] J.H. Schattka, D. Shchukin, G. Jia, J.M. Antonietti, R.A. Caruso, Chem. Mater. 14 (2002) 5103–5108.
[40] D. Jing, Y. Zhang, L. Guo, Chem. Phys. Lett. 415 (2005) 74–79.
[41] X. Wang, R.A. Caruso, J. Mater. Chem. 21 (2011) 20–28.
[42] X. Wang, J.C. Yu, H.Y. Yip, L. Wu, P.K. Wong, S.Y. Lai, Chem. Eur. J. 11 (2005) 2997–3004.
[43] M. Anderson, H. Birkedal, N.R. Franklin, T. Ostomel, S. Boettcher, A.C. Palmqvist, G.D. Stucky, Chem. Mater. 17 (2005) 1409–1415.
[44] Z. Ding, X.J. Hu, G.Q. Lu, P.L. Yue, P.F. Greenfield, Langmuir 16 (2000) 6216–6222.
[45] K. Wang, B. Yao, M.A. Morris, J.D. Holmes, Chem. Mater. 17 (2005) 4825–4831.
[46] D.S. Kim, S.Y. Kwak, Environ. Sci. Technol. 43 (2009) 148–151.
[47] G.S. Li, J.C. Yu, J. Zhu, Y. Cao, Microporous Mesoporous Mater. 106 (2007) 278–283.
[48] M.C. Mascolo, G. Dell'Agli, G. Mascolo, Microporous Mesoporous Mater. 132 (2010) 196–200.
[49] D. Vorkapic, T. Matsoukas, J. Am. Ceram. Soc. 81 (1998) 2815–2820.
[50] J. Livage, M. Henry, C. Sanchez, Prog. Solid State Chem. 18 (1988) 259–341.
[51] G.W. Scherer, J. Am. Ceram. Soc. 73 (1990) 3–14.